WSRC-MS-20000-00403

Development of Mechanical Properties Database of A 285 Steel for Structural Analysis of Waste Tanks

A. J. Duncan, K. H. Subramanian, and R. L. Sindelar
Westinghouse Savannah River Company
Aiken, SC 29808

K. Miller, A. P. Reynolds, and Y. J. Chao
University of South Carolina
Columbia, SC 29208

This document was prepared in conjunction with work accomplished under Contract No. DE-AC09-96SR18500 with the U.S. Department of Energy.

DISCLAIMER

This report was prepared as an account of work sponsored by an agency of the United States Government. Neither the United States Government nor any agency thereof, nor any of their employees, makes any warranty, express or implied, or assumes any legal liability or responsibility for the accuracy, completeness, or usefulness of any information, apparatus, product or process disclosed, or represents that its use would not infringe privately owned rights. Reference herein to any specific commercial product, process or service by trade name, trademark, manufacturer, or otherwise does not necessarily constitute or imply its endorsement, recommendation, or favoring by the United States Government or any agency thereof. The views and opinions of authors expressed herein do not necessarily state or reflect those of the United States Government or any agency thereof.

This report has been reproduced directly from the best available copy.

Available for sale to the public, in paper, from: U.S. Department of Commerce, National Technical Information Service, 5285 Port Royal Road, Springfield, VA 22161, phone: (800) 553-6847, fax: (703) 605-6900, email: orders@ntis.fedworld.gov online ordering: http://www.ntis.gov/support/ordering.htm

Available electronically at http://www.osti.gov/bridge/

Available for a processing fee to U.S. Department of Energy and its contractors, in paper, from: U.S. Department of Energy, Office of Scientific and Technical Information, P.O. Box 62, Oak Ridge, TN 37831-0062, phone: (865) 576-8401, fax: (865) 576-5728, email: reports@adonis.osti.gov

Abstract

A statistically-designed test matrix has been developed to govern test conditions to measure the fracture toughness properties of A285 carbon steel. The effects of several variables on ductile tearing were investigated. The database of J-resistance (J-R) curves are applicable to flaw stability analyses in waste storage tanks constructed in the 1950's at the Savannah River Site (SRS).

J-Integral toughness tests were conducted as a function of composition, grain size, orientation, operating temperature and loading rate to measure fracture properties. Composition and grain size were selected over ranges based on available heats of new and 1950's vintage material from archival site sources. The J-R curve was observed to be highly sensitive to carbon content and the crack plane orientation with respect to the rolling direction of the plate. No effect of temperature (T) and thickness (t) on the J-R curves was observed for the range of test conditions (288 £ T £ 300 K, 12.7 £ t £ 22.2 mm). The loading rate was held constant at 0.77 MPa-m$^{0.5}$/sec, but will be varied in future work

of this program. The specimen dimensions were designed to simulate the thickness of tank wall regions in the structure and to a width that insured back end constraint after crack extension up to several mm.

Keywords: J-Integral, Fracture Toughness, A285 Steel, Waste Tanks

Introduction

Background

The waste storage tanks at SRS were manufactured from A285-50T Grade B carbon steel in the early 1950's and have been in operation since that time. This steel was produced from semi-killed ingots and hot rolled into plates ranging in thickness from 12.7 to 22.2 mm. During service several tanks have developed flaws by stress corrosion cracking, currently inhibited by rigorous chemistry controls. In addition, these tanks are operated above ambient temperatures between 305 and 336 K (and never below 294 K) to avoid the potential for brittle fracture behavior of the steel. Accurate flaw stability analysis, must therefore consider the ductile tearing behavior of this material at these conditions.

A database of fracture toughness properties is being developed for A285 carbon steel for application to flaw stability analysis of waste storage tanks at SRS. Previous flaw stability analyses used lower bound fracture toughness properties from a cutoff in the J-R curves, but the effects of composition, orientation or temperature on properties were not fully investigated [,]. To provide for material and flaw-specific stability analysis and improve the accuracy of operational limits, an extensive testing program was developed to quantify the effects of material and service condition on the fracture properties. The fracture properties are J-R curves in accordance with ASTM Standard Test Method for Measurement of Fracture Toughness (E 1820) [3].

Test Matrix

A285 carbon steel demonstrates a wide variation of fracture properties depending on composition, microstructure, orientation and other factors [4,5,]. If the effects of these factors are known, material-specific flaw stability analyses may be conducted in order to improve the accuracy for operational limits. To achieve, a statistical test design was prepared to investigate the impact of composition, orientation, microstructure and other environmental parameters on the fracture properties of A285 carbon steels. Variables were defined at levels relevant to the material and test conditions for waste storage tanks. Several heats of A285 steel were acquired with a variety of compositions and plate thicknesses. The compositional span of the heats and specific compositions of heats in question are included in Table 1 along with grain size and yield strengths from the materials certificate. A total of twelve heats were acquired, to make up the test matrix, which represented a distribution throughout the compositional range shown in Table 1.

A quadratic model, based on the test parameters to be investigated was developed and a statistically designed test matrix was generated in order to predict mechanical properties as function of composition, microstructure, geometry, loading rate and temperature. The resultant matrix provided over 100 trials for the measurement of mechanical properties as a function of these variables. The mechanical properties of primary interest are (1) fracture toughness and (2) tensile properties. In this study, the initial 15 fracture toughness tests are reported along with preliminary observations and data analysis. Experimental variables of the test matrix, shown in Table 2, include thickness, orientation, and temperature.

Property Database

Elastic-plastic fracture mechanics methodologies with a ductile tearing instability criterion are needed to perform flaw stability analyses for waste tanks at SRS. For this analysis, J cutoff values are required for inputs, so J-Integral toughness testing was used to compile material J-R curves and determine J at a specified cutoff value (i.e., 3mm) from a power law fit to data. Statistical confidence intervals were compiled for J cutoff values of samples tested under similar conditions. J_{IC} was also determined from the power law fit of the J-R curves for comparison.

Testing Methods

Microstuctural Analysis

Samples were characterized using optical metallography. Ferrite grain sizes were measured in each orientation using the linear intercept method in accordance with ASTM Test Methods for Determining Average Grain Size Using Semiautomatic and Automatic Image Analysis (E 1382) [6]. The grain size reported is averaged over three orientations. Fracture surfaces were analyzed using scanning electron microscopy.

Specimen Design

Fracture toughness testing was performed on compact tension specimens of ASTM standard geometry shown in Figure 1. The specimens were machined in nominal configuration for a specimen of varying thickness (B) from 12.7 to 22.2 mm. The nominal specimen width (W) of 63.5 mm was chosen in order to allow for measurement of valid J at large crack extensions, in accordance with ASTM E 1820. However, the thickness was not increased for two reasons: (1) thickness was limited to the maximum section thickness of the storage tanks, 22.2 mm, (2) many of the heats available for testing have a maximum plate thickness of less than 20 mm. In addition, all dimensions were kept constant to facilitate machining.

Testing

Fracture toughness tests were conducted and J-R curves were derived for each of the specimens, as prescribed by ASTM E 1820. Crack length measurements were made by Direct Current Potential Drop (DCPD) and unloading compliance (UC), depending upon sample. All tests were performed corresponding to a stress intensity loading rate of 0.7 (ksi-$\sqrt{}$ in) /sec. The load line crack opening displacement was measured with an inboard clip gage attached to front notches at the load line. After testing, optical crack length measurements were made and used to transcribe experimental crack length data as per ASTM E 1820. The transcribed crack length data were used to calculate J deformation (J_{def}) in accordance with ASTM E 1820.

Results and Discussion

Microstructures

The microstructure of each heat consists of ferrite grains with intergranular pearlite. All three of these heats exhibited, to some degree, banding of pearlite, which is typical in hot rolled plate. An example of pearlite banding is shown in Figure 2. This condition has been attributed to manganese segregation in steels, but may also be caused by precipitation of non-metallic inclusions or hot rolling at low finishing temperatures and cooling rates [7]. The effects of banding and/or inclusions on mechanical properties can vary depending on orientation, morphology and continuity. In general, the presence of banding has been observed to lower the upper shelf fracture energy while decreasing the ductile to brittle transition temperature in charpy impact tests [8]. The microstructures of all three heats (E400, 382835 and 1A434) are shown in Figure 3 a, b and c in each orientation.

Figure 4 illustrates how the fracture surfaces of these steels differ with orientation in the same heat. Figure 4a shows the fracture surface of an E400 specimen in the T-L orientation. Delaminations, coincidental with pearlite bands, divide the crack plane similar to a crack divider orientation. This differs from the less directional void growth in the L-T orientation (Figure 4b), where the pearlite banding is less continuous. The specific impact of either pearlitic banding or non-metallic inclusions on fracture behavior in these steels is not been distinguished in this study. However, it is expected that both effect the operating fracture mechanisms during failure. One study on banded steel [6] determined that the effect of inclusion content had a larger impact on the reduction of upper-shelf charpy fracture energy than banding.

J-R Curves

J-R curves are shown for each, the T-L and L-T orientation of heat E400, in Figure 5 and Figure 6 respectively. It is seen that J_{def} values for the T-L orientation show a mean of approximately 328 kJ/m^2 at 3 mm of crack extension. In

comparison, the J_{def} values for the L-T orientation show a mean of approximately 580 kJ/m^2 at 3 mm. This indicates a steeper J-R curve for the L-T orientation as expected. A pronounced orientation effect is seen in Figure 7. Specifically, the J-R curves from L-T oriented specimens are shown to exhibit a higher resistance to fracture than T-L oriented specimens. This may be related to the presence of continuous delaminations during crack growth in the T-L orientation that cause a reduced resistance to fracture.

Testing in the low toughness T-L orientation showed remarkable reproducibility. In the high toughness L-T orientation, however, the J-R curves have greater scatter. The E400L6 specimen was not sidegrooved, and hence, is expected have a higher J-R curve due to lower constraint. Both E400L4 and E400L8 were tested using unloading compliance, which may have contributed to scatter. Sample E400L8 was 20% side-grooved and consequently exhibited less crack tunneling. Additional scatter could be a result of microstructural discontinuities not encountered in the T-L orientation (i.e., banding or inclusion distribution). Test temperature variation and thickness variation had a minimal effect on the J-R curves in the their respective tested ranges. This is not surprising considering the narrow range of both thickness and temperature tested.

Figure 8 shows the effect of carbon content on J-based behavior. These data include preliminary data from heats 1A434 and 382835 in the T-L orientation. It can be seen that a higher carbon content results in lower J-R curve behavior. Further tests will be done to specify carbon effects on J-R curve behavior and fracture toughness and their implications on waste tank integrity.

Data Analysis

J_{3mm} Analysis

The J-deformation value at a crack extension of 3mm was chosen as a point of comparison in order to accredit extensive stable crack growth as a result of plasticity. In addition, crack extension of 3mm ensures validity within plastic zone size restrictions. The values of J at 3 mm were determined (extrapolated when necessary) from a power law fit to data within ASTM E 1820 validity. The results of which are shown in Table 3 and Table 4, for the T-L and L-T orientations, respectively. Each data set was fit to a normal distribution; the mean and standard deviation (along with the coefficient of variation) are also included in Table 3 and Table 4. The results for several one-sided tolerance intervals are provided in these tables. With 90% confidence, 90% of the population of toughness results for E400 in the T-L orientation has a J value of greater than 308 kJ/m^2. With 90% confidence, 90% of the population of toughness results for E400 in the L-T orientation has a J value of greater than 462 kJ/m^2. Although the sample sizes are small, and that an increased sample size would provide a reduced tolerance interval, the critical difference between the two distributions is the standard deviation. Comparing the coefficient of variations (COV) of each distribution demonstrates this point. The COV is the standard deviation normalized by the mean. When comparing the COV from each distribution it is apparent that the COV for the L-T orientation is almost 4 times that of the T-L orientation. This is a direct result of the increased scatter in the J-R curves discussed above.

J_{IC} Analysis

J_{IC} values were derived as prescribed by ASTM E 1820, using a slope of 2 and yield strengths from the materials certificates for the blunting line construction. The J_{IC} results are shown in Table 5. Samples E400L4 and E400T4 show a much higher J_{Ic} than their DCPD counterparts in each respective orientation, due to load relaxation during the unloading cycles during the test. However, sample E400L8 (also measured by unloading compliance), used repeated unloading cycles at each interval to diminish the effects of load relaxation. In addition, E400L8 was 20% sidegrooved to prevent extensive crack tunneling as was seen with other samples. It is seen that the L-T orientation exhibits higher J_{IC}.

Summary

J-Integral testing was performed on A285 semi-killed, hot rolled plates to determine the effect of composition,

microstructure and orientation on the fracture behavior of carbon steel for storage tanks at the Savannah River Site. The preliminary findings in comparing the toughness results from the initial tests are the following:

- Strong dependency on orientation (Lower toughness in T-L than in L-T orientation)
- Strong dependency on carbon content (lower toughness with increased carbon content)
- Negligible sensitivity to temperature (between 288 to 300 K)
- Negligible dependency on thickness in testing range
- A wider distribution of properties in L-T oriented specimens

These conclusions are drawn based primarily on comparison of the heat E400 J-R curves. Toughness behavior as a function of each variable will be further tested to ensure results.

Additional fracture toughness tests will be performed and also tensile tests to determine J_{IC} values. When data acquisition from the entire test matrix is complete, the data will be used to compile a predictive model for flaw behavior in storage tanks.

Acknowledgements

Our colleagues, Drs Bruce J. Wiersma, Poh-Sang Lam and Steven P. Harris Jr. are gratefully acknowledged for their contribution to this study. Dr. Wiersma is the lead investigator for service effects to the storage tanks and has provided much of the background work for this study. Dr. Lam reviewed this manuscript. Dr. Harris generated the statistically designed test matrix referred to in this study. This work was funded by the U. S. Department of Energy under contract No. DE-AC09-96SR18500.

References

1. Sindelar, R. L., Lam, P. S., Caskey, Jr., G. R. and Woo, L. Y., "Flaw Stability in Mild Steel Tanks in the Upper Shelf Ductile Range-Part I: Mechanical Properties," ASME J. Pressure Vessel Technol., 122, May (2000) to be published.
2. Lam, P-S., and Sindelar, R. L., "Flaw Stability in Mild Steel Tanks in the Upper Shelf Ductile Range-Part II: J-Integral Based Fracture Analysis" ASME J. Pressure Vessel Technol., 122, May (2000) to be published.
3. "Standard Test Method for Measurement of Fracture Toughness," ASTM Standard E 1820 - 99, Annual Book of ASTM Standards, 3.01 (1999).
4. Burns, K. W., and Pickering, F. B., "Deformation and Fracture of Ferrite-Pearlite Structures," J. Iron and Steel Inst., Nov. (1964), pp. 899-906.
5. Boulger, F. W., and Frazier, R. H., "The Influence of Carbon and Manganese on the Properties of Semikilled Hot Rolled Steel," J. Metals, Trans. AIME, May (1954), pp. 645-652.
6. "Test Methods for Determining Average Grain Size Using Semiautomatic and Automatic Image Analysis," ASTM Standard E 1382 - 97, Annual Book of ASTM Standards, 3.01 (1999).
7. Grange, R. A., "Effects of Microstructural Banding in Steel," Metallurgical Trans. 2, Feb. (1971), pp. 417-426.
8. Shanmugam, P., Pathak, S. D., "Some Studies on the Impact Behavior of Banded Microalloyed Steel," Engineering Fracture Mechanics, 53 [6] (1996), pp. 991-1005.

Table 1: Compostions, Grain Size and Yield Streghts of Selected Heats

Heat	C (wt%)	Mn (wt%)	P (wt%)	S (wt%)	Grain (μm)	σ_{ys} (MPa)
A285*	0.05-0.023	0.35-0.9	0.005-0.035	0.005-0.032		
E400	0.18	0.43	0.009	0.026	51.2	290
1A434	0.082	0.676	0.017	0.011	52.1	317
382835	0.15	0.84	0.005	0.012	50.6	308

* Range of compositions considered for study

Table 2: Test Matrix and Test Conditions

Heat	Sample	Thickness (mm)	Side Groove	Temp (K)	Orient.
E400	L1	12.7	10%	294	L-T
E400	L2	12.7	10%	294	L-T
E400	L3	15.9	10%	294	L-T
E400	L4	15.9	10%	294	L-T
E400	L6	15.9	0%	300	L-T
E400	L8	15.9	20%	294	L-T
E400	L9	15.9	20%	294	L-T
E400	L10	15.9	20%	294	L-T
E400	T1	12.7	10%	294	T-L
E400	T2	12.7	10%	300	T-L
E400	T3	15.9	10%	294	T-L
E400	T4	15.9	10%	294	T-L
E400	T5	15.9	20%	300	T-L
1A434	9	22.2	10%	288	T-L
382835	15	19.0	10%	288	T-L

Table 3: J_{3mm} Data for Heat E400, T-L Orientation

Sample	Technique	J_{3mm} (kJ/m^2)	Mean	Std Dev	One-Sided %p / Tolerance	OneSided Minimum
E400T1	DCPD	335	328.2	7	90/90	308
E400T2	DCPD	334			95/90	304
E400T3	DCPD	326		COV	90/95	303
E400T4	UC	329		2.2%	95/95	298
E400T5	DCPD	317				

Table 4: J_{3mm} Data for Heat E400, L-T Orientation

Sample	Technique	J_{3mm}	Mean	Std Dev	One-Sided %p / Tolerance	OneSided Minimum
E400L1	DCPD	625	580	47	90/90	462
E400L2	DCPD	583			90/95	434
E400L4	UC	612			95/90	438
E400L6	DCPD	801		COV	95/95	405
E400L8	UC	532		8%		
E400L9	DCPD	617				
E400L10	DCPD	513				

Table 5: J_{IC} Results for Heat E400 (L = L-T Orientation, T = T-L Orientation)

Sample	J (kJ/m^2)
E400L1	172
E400L2	141
E400L4	387
E400L6	266
E400L8	220
E400L9	141
E400L10	126
E400T1	99
E400T2	74
E400T3	42
E400T4	171
E400T5	87

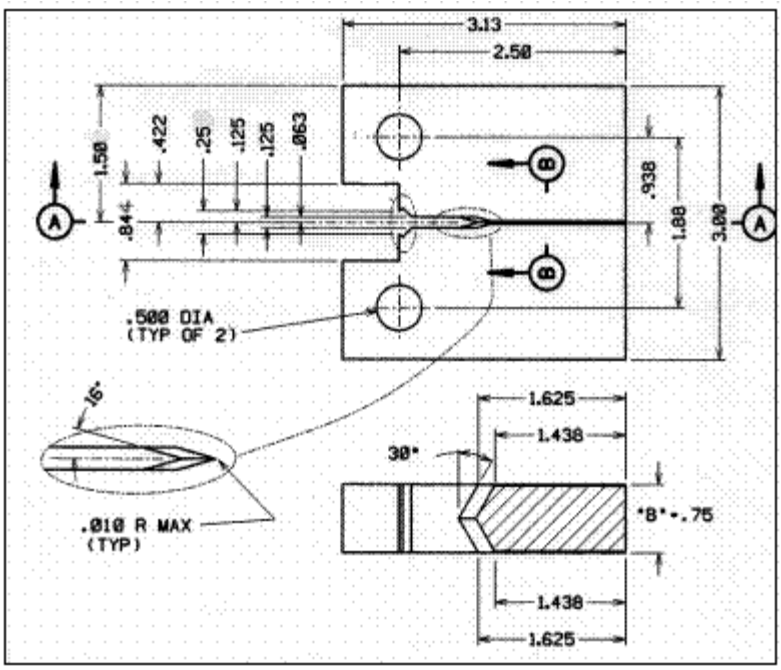

Figure 1: Nominal Compact Tension Specimen Design

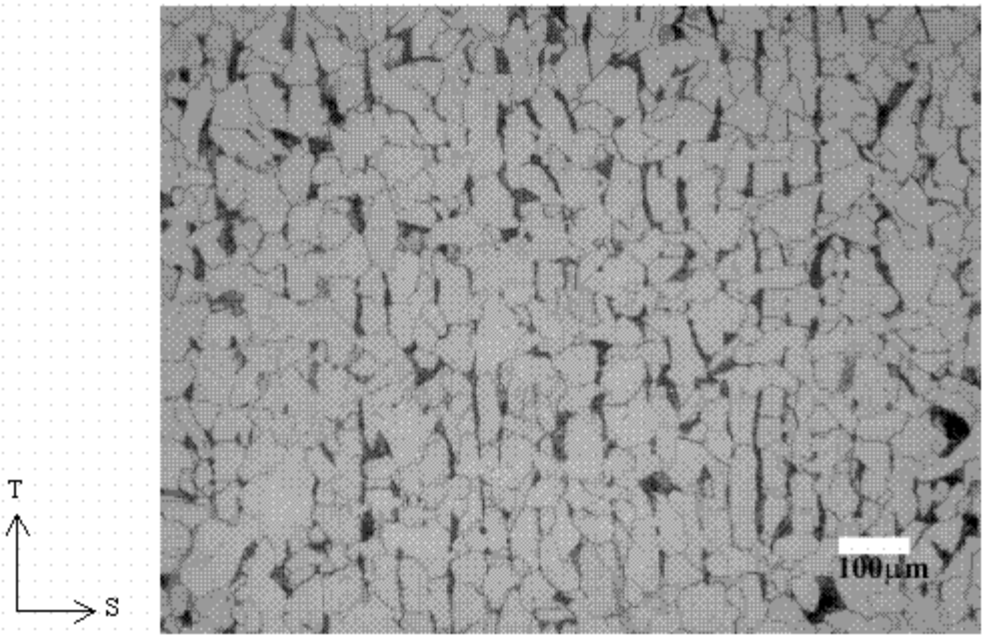

Figure 2: Example of Pearlite Bands Observed in Heat E400

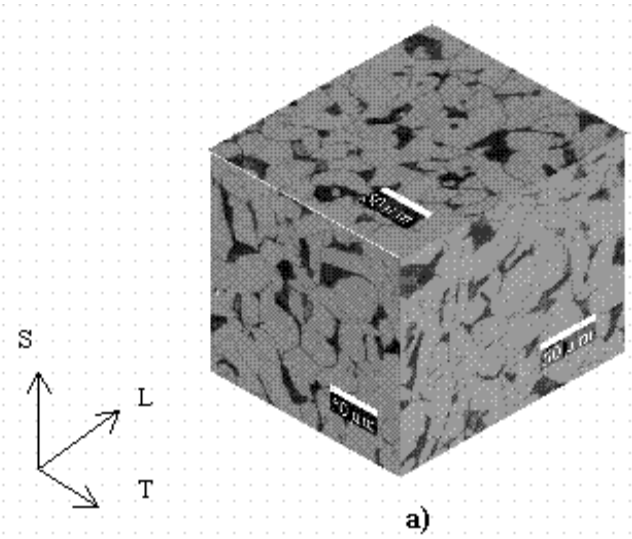

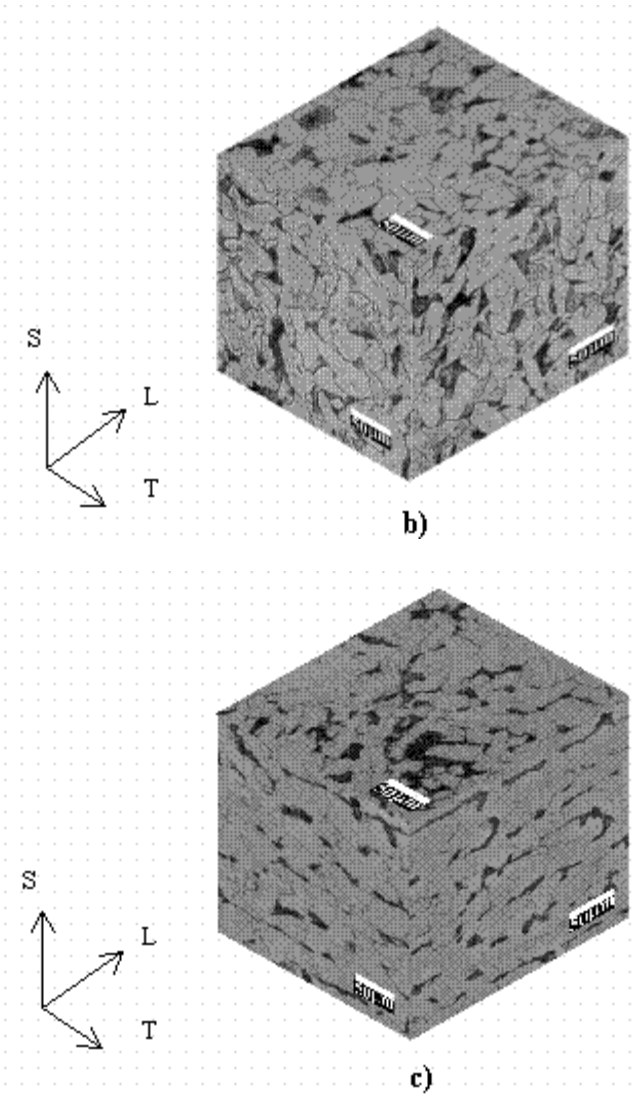

Figure 3: Microstructure of Heats a) E400, b) 382835 and c) 1A434

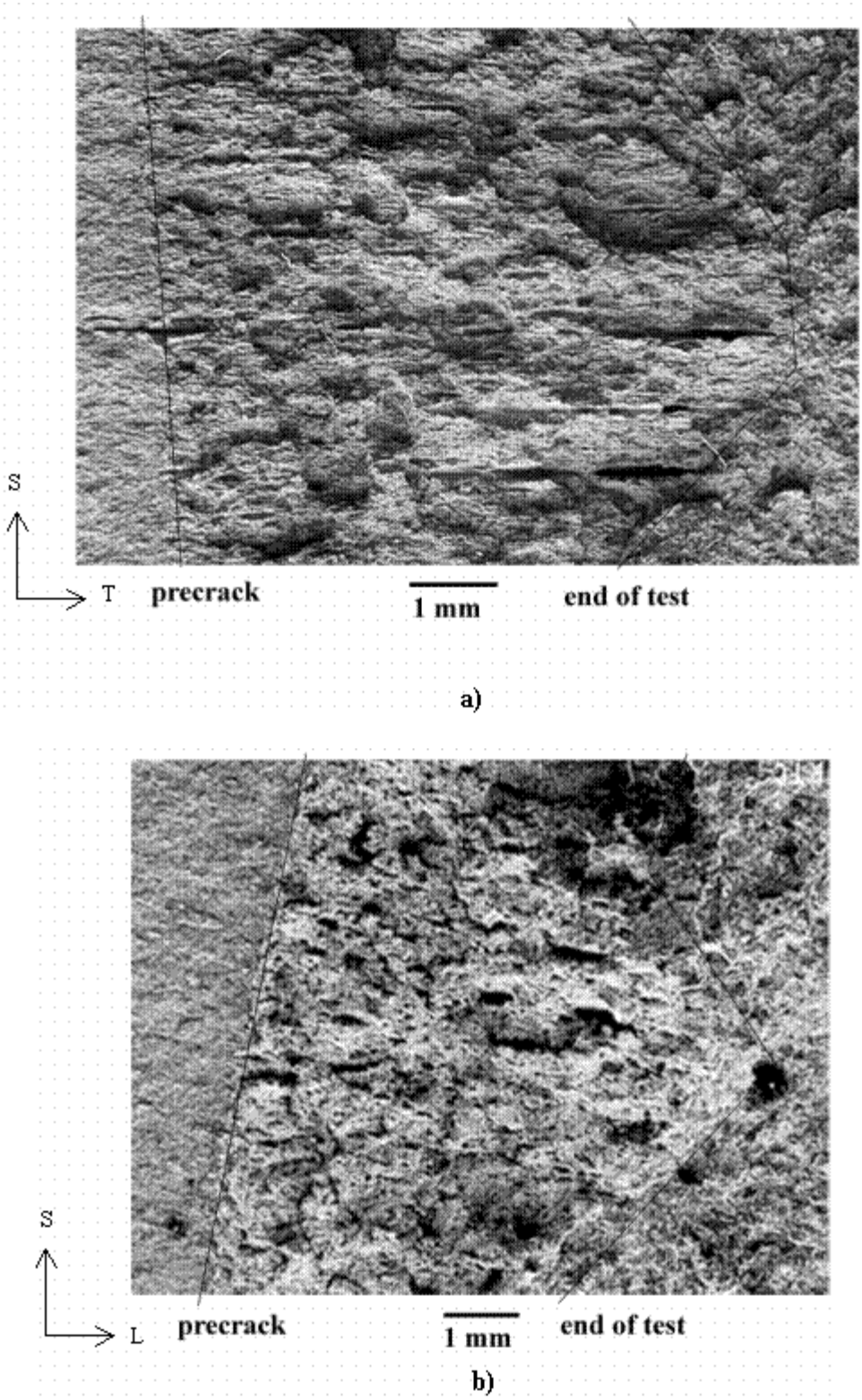

Figure 4: SEM Micrograph of the Fracture Surfaces of E400 C(T) Specimens in the a) T-L and b) L-T Orientations

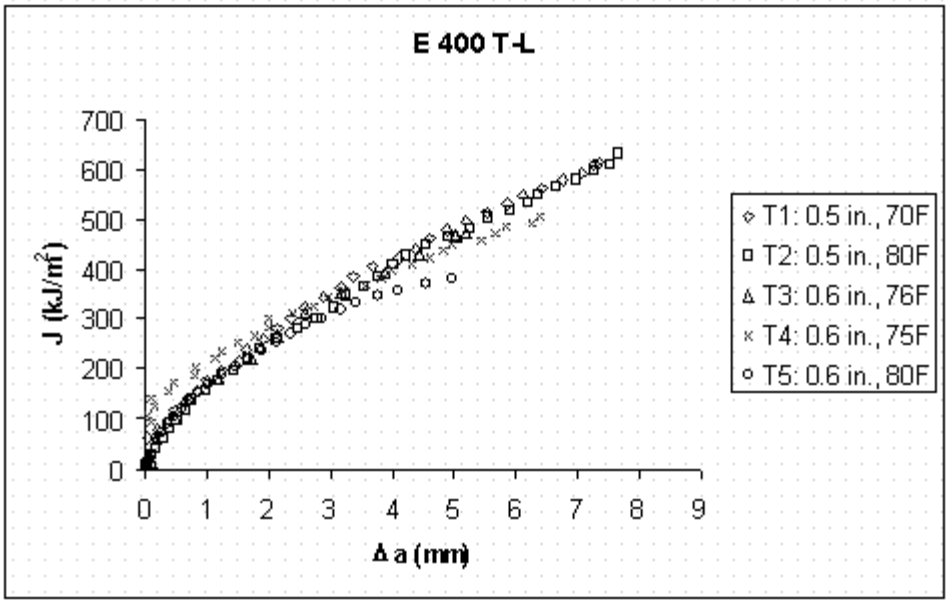

Figure 5: J-R Curves for Heat E400 T-L Orientation (Test Temperature and Sample Thickness shown)

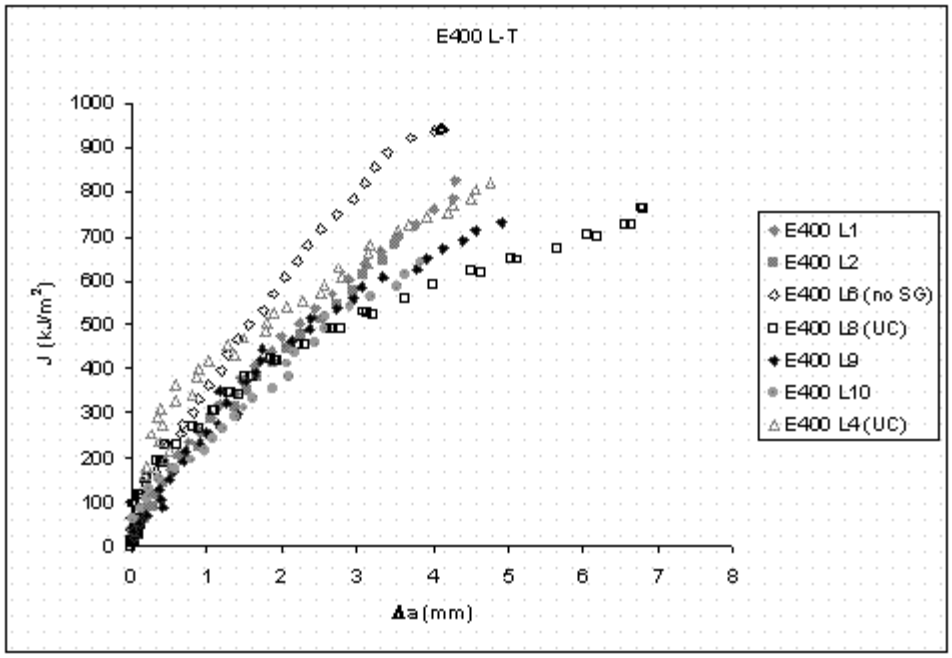

Figure 6: J-R Curves for Heat E400 L-T Orientation (Test Variances Shown in Legend)

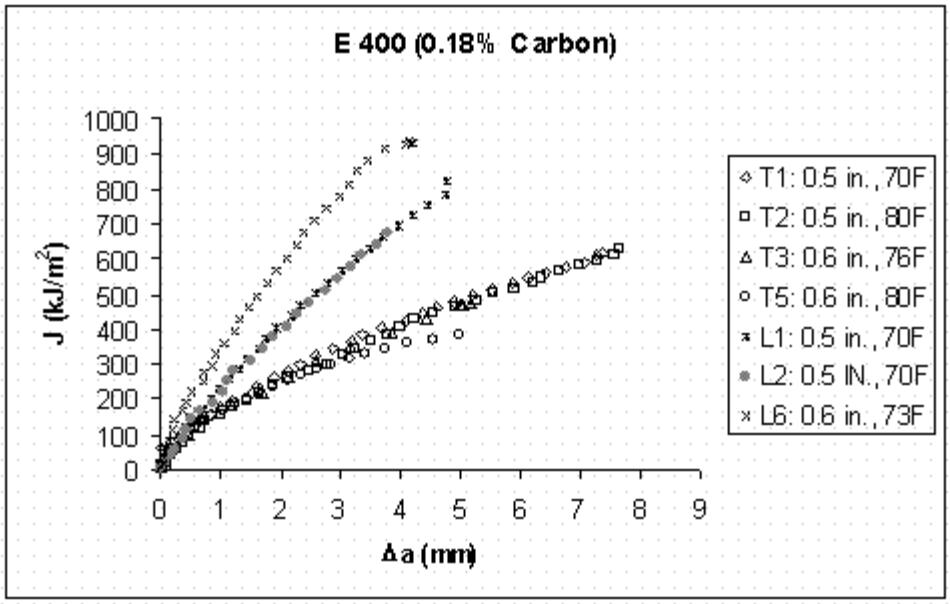

Figure 7: J-R Curve Variability with Orientation for Heat E400 (Test Temperature and Sample Thickness shown in legend)

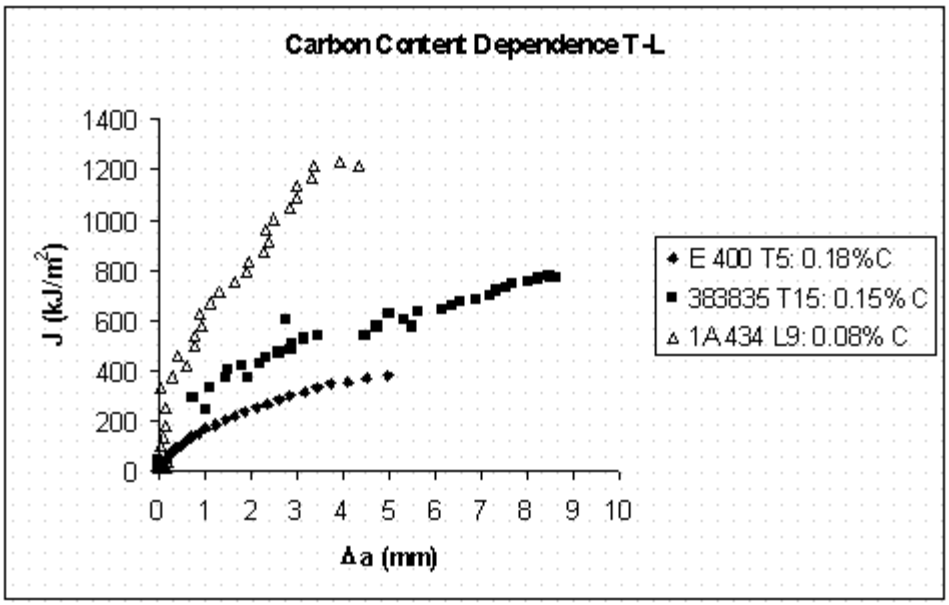

Figure 8: Preliminary J-R Curve Dependence on Carbon Content in T-L Orientation